Accurate dynamics of microscopic filaments using "caterpillar" Oseen hydrodynamics

Aimee G. Bailey,[1,*] Christopher P. Lowe,[2] I. Pagonabarraga,[3] and M. Cosentino Lagomarsino[4,5]

[1]*Department of Physics, Imperial College London, Department of Physics, Exhibition Road, London SW7 2AZ, United Kingdom*

[2]*HIMS, Universiteit van Amsterdam, Nieuwe Achtergracht 166, 1018 WV Amsterdam, The Netherlands*

[3]*Departament de Fisica Fonamental, Universitat de Barcelona, Carrer Marti i Franques 1, 08028-Barcelona, Spain*

[4]*Universit degli Studi di Milano, Dip. Fisica. Via Celoria 16, 20133 Milano, Italy*

[5]*INFN, Milano Via Celoria 16, 20133 Milano, Italy*

(Dated: April 22, 2009)

Abstract

Microscopic semi-flexible filaments suspended in a viscous fluid are widely encountered in biophysical problems. The classic example is the flagella used by micro-organisms to generate propulsion. Simulating the dynamics of these filaments numerically is complicated because of the coupling between the motion of the filament and that of the surrounding fluid. An attractive idea is to simplify this coupling by modeling the fluid motion by using Stokeslets distributed at equal intervals along the model filament. The question then is, how well does this represent reality? We show that, with an appropriate choice of the hydrodynamic radius, the answer to this question is - very well. The model reproduces the variation of the friction along the length characteristic of a slender cylindrical filament, without requiring an explicit surface. This is true, however, only if the hydrodynamic radii take specific values and that they differ in the parallel and perpendicular directions. Having demonstrated this, we use the model to compare with analytic theory of filament deformation and rotation in the small deformation limit. (PACS: 87.16.Ka, 05.45.a, 46.32.+x, 47.15.Gf)

*aimee.bailey06@imperial.ac.uk

I. INTRODUCTION

Microscopic biological filaments moving in a low Reynolds number environment are fundamental to the functioning of organisms. Typical examples include flagella and cilia in the field of micro-organism motility [1–3]. Understanding the interplay between the filament and its surroundings has notable biological implications in the context of the incipient stages of life [4], not to mention the design and development of fabricated micro-swimmers [1, 5]. Other biological constituents whose statics and dynamics are critical in cellular function include biopolymers such as microtubules [6, 7]. All of these examples have one common feature: the biological component is relatively stiff and has a high aspect ratio (the length greatly exceeding the width). Mechanically these systems exhibit behavior indicative of flexible filaments. The collective complexity of the molecular structure manifests itself simply as an effective bending elasticity. This being the case, one can gain insight by studying inextensible, flexible filaments, which serve as a surprisingly good approximation to more realistic descriptions [8].

The interesting, counterintuitive behavior of biological systems is often due to the interaction of the body with its viscous environment [1, 9, 10]. For example, a one-armed swimmer tries to propel itself by waving a stiff appendage, but it will go nowhere in the absence of inertia (low Reynolds number). However, this is a perfectly viable means of propelling one's own body in a swimming pool (high Reynolds number). Resistive force theory [11] is frequently used to mimic this interplay, approximating the interaction as a local relationship between the force and velocity. For theoretical investigations, it is useful in that it is more frequently analytically tractable. Hydrodynamic effects, however, are long-range and scale inversely with distance, rendering this local description quite a limited one. In fact, the very simplest example – a flexible filament in a static external field – yields rich dynamic behavior that is impossible to predict using resistive force theory [9, 12, 13]. Not surprisingly, incorporating the coupling between the body and the fluid is also significant for more sophisticated systems, such as the growth of liquid crystals [14].

Significant progress has been made analytically using the Kratky-Porod wormlike chain model, in which the filament is treated as a continuous elastic curve with constant length [15–17]. Differential equations for systems evolving under elasticity typically involve high order spatial derivatives and contain non-linear terms. The dynamics of a 2D curve with the very

simplest elastic bending energy (quadratic in curvature) is non-linear and depends on the 6^{th} order spatial derivative of the positions [15]. This is the most basic conceivable example and already the mathematical complications are daunting. Categorically, the equations of motion, either the full or a linearized version, have to be discretized and integrated numerically to realize the dynamics. This in itself is a formidable task. Only sophisticated techniques such as pseudospectral methods correctly treat high order derivatives to obtain an accurate and numerically stable simulation [15, 17]. This is not to mention that many of these studies use resistive force theory, which we have already pointed out is limited. The above complications are prohibitive but only arise because the filament is described by a continuous curve and an analytical path is pursued. If we were to instead use a discrete description to develop an accurate computational tool, speculative simulations exploring complex configurational space could be very easily be carried out.

With this in mind, here we describe a simple and computationally efficient simulation model of a flexible filament immersed in a viscous fluid. The various force contributions are described in detail. In a simulation model, at a small additional computational cost, one is not limited to resistive force theory but can use the more accurate Stokesian description that takes into account the body-fluid coupling. Representing a filament as a sequence of 'Stokeslets', or point forces acting on the fluid, is not new [9, 12, 18, 19]; however, we show in this article that agreement between slender body theory and the continuum limit of the discrete Stokesian hydrodynamic force is conditional on the choice of a tensor hydrodynamic radius with specific values relative to the bead spacing. This is in contrast to previous work where the hydrodynamic radius is set to exactly half of the bead spacing, which is referred to as the "shish kebab" model [20]. We show that by choosing the hydrodynamic radius appropriately, we are not limited to infinitely slender bodies; instead, we can accurately simulate systems that have a realistic aspect ratio, such as a flagella which can have a diameter of a few percents of the filament length [3].

II. FILAMENT MODEL

We describe a model filament as a collection of equally spaced points along a curve. All forces and masses are concentrated at the site locations, which we will refer to as *beads* using conventional nomenclature. Three types of forces – elasticity, hydrodynamics, and tension

– form the basis of the model. External forces relevant for a specific application can easily be added.

A. Elastic forces

The filament evolving under elasticity will be penalized for deviation from the lowest energy conformation. If we take the ground state of the elastic filament to be a straight line, the continuous equation for the elastic energy is an integral over the entire contour length of the square of the curvature (κ) [21].

$$U_e = \frac{\alpha}{2} \int_{-l}^{l} \left| \frac{\partial^2 \mathbf{r}}{\partial s^2} \right|^2 ds = \frac{\alpha}{2} \int_{-l}^{l} \kappa^2 ds \tag{1}$$

The position of the filament is denoted by $\mathbf{r}$. The contour length (s) spans from $-l$ to l, where $L = 2l$. The constant α is the elastic flexure, or bending rigidity. This result is from continuum elasticity theory, but our filament is actually represented as a discrete collection of connected beads, separated by a spacing of $b = L/(n-1)$. The variable θ is the deviation of the tangent from the straight line of adjacent segments at bead i, given by

$$\cos(\theta_i) = \frac{\mathbf{r}_{i-1,i} \cdot \mathbf{r}_{i,i+1}}{b^2} \ , \tag{2}$$

where $\mathbf{r}_{ij} = \mathbf{r}_i - \mathbf{r}_j$. Relating the local radius of curvature to the angle θ by the cosine rule, we have

$$\kappa_i^2 = \frac{2}{b^2} \left(1 - \cos(\theta_i)\right). \tag{3}$$

Using this relationship, the discrete counterpart of Eq. (1) is

$$U_e = \frac{\alpha}{b} \sum_{i=1}^{n-1} \left(1 - \cos(\theta_i)\right). \tag{4}$$

The elastic forces are the gradient of Eq. (4) with respect to position.

In our model the filament has a fixed segment length, meaning b is constant (see Sec. II C). Therefore, no elastic energy can be stored in the form of axial extension/compression. The filament simply has an energetic incentive to remain straight. This is analogous to writing Eq. (1) with a Lagrange multiplier term to enforce local length constraints. Experiments measuring force-extension curves indicate the Kratky-Porod wormlike chain model is a good description of biofilaments and proteins [22–25]. Therefore, our combination of a bending penalty plus length constraints is justified.

B. Hydrodynamic forces

In order to mimic the interaction of the filament submersed in a viscous fluid, we need to include hydrodynamic forces. Solving the fluid flow equations exactly with a stick boundary condition in a dynamic simulation, during which the shape evolves, is a computationally daunting task. Alternatively, resistive force theory [11] provides a much simplified description, but there are many instances where one cannot neglect the hydrodynamic coupling [12, 14]. Conveniently, we will show that the solution of the flow equations can be approximated by treating the continuous object as a collection of discrete Stokeslets, or point forces. At arbitrarily high Stokeslet density, the continuous form of the object is recovered. For example, the hydrodynamic force acting on our filament can be modeled using a line of sufficiently numerous Stokeslets to recreate the behavior of a continuous curve. An advantage of this methodology, in addition to being computationally tractable for simulations over long timescales, is that unbounded geometries can be considered.

The hydrodynamic force in our model is defined by

$$\mathbf{F}_{iH} = -\gamma_0 \left(\mathbf{v}_i - \mathbf{v}_{iH} \right). \tag{5}$$

The constant γ_0 is the bead friction, where $\gamma_0 = 6\pi\eta a$. The constants η and a are the fluid viscosity and the hydrodynamic bead radius, respectively. Note that a is not a real radius, in that the beads in the model have no spacial extension. Rather, it is a parameter determining the friction strength. The term $\mathbf{v}_i$ is the velocity of the filament at bead i, and $\mathbf{v}_{iH}$ is the velocity of the fluid at the same location. We have written Eq. (5) with a scalar bead friction for now, although we show in the following sections that in fact γ_0 – and therefore the hydrodynamic radius a – must be a tensor to recover results from slender body theory.

Using the Stokeslet form for the fluid velocity, we have

$$\mathbf{v}_{iH} = \frac{1}{8\pi\eta} \sum_{i \neq j} \left(\frac{\mathbf{F}_j}{|r_{ij}|} + \mathbf{F}_j \cdot \frac{\mathbf{r}_{ij}\mathbf{r}_{ij}}{|r_{ij}|^3} \right), \tag{6}$$

which gives the following hydrodynamic force:

$$\mathbf{F}_{iH} = -\gamma_0 \mathbf{v}_i + \frac{\gamma_0}{8\pi\eta} \sum_{i \neq j} \left(\frac{\mathbf{F}_j}{|r_{ij}|} + \mathbf{F}_j \cdot \frac{\mathbf{r}_{ij}\mathbf{r}_{ij}}{|r_{ij}|^3} \right). \tag{7}$$

$\mathbf{F}_i$ is the force on bead i. Eq. (6) is derived by eliminating the convective terms in the Navier-Stokes equations. In other words, it is consistent with the Reynolds number being low, with fluid inertia neglected.

C. Length constraints

In order to fix the contour length, we use SHAKE methodology to incorporate length constraints in a dynamic simulation [26]. The distance between all connected beads is held at a constant value to within a predefined degree of accuracy. For all results presented here, we set the accuracy to be a relative bead separation $|\mathbf{r}_{ij}|/b$ of within 10^{-12}. Using SHAKE methodology, there is an array of numerical recipes one can use to calculate the Lagrange multipliers that make up the constraint forces. For a linear geometry in which each bead is connected to at most two nearest neighbors, such as the geometry we are considering here, we use and recommend MILC SHAKE, which can be orders of magnitude faster than SHAKE iteration [27].

D. Integrating the equations of motion

Now that all forces have been identified, what remains to be specified is an appropriate integration scheme to evolve the equations of motion in a dynamic simulation. With velocity-dependent forces present, one cannot use the standard velocity Verlet algorithm [28]. Instead, one can derive an update scheme using the Trotter factorization of the Liouville propagator, the same method used to derive the reversible, multiple time scale, molecular dynamics scheme RESPA [29]. Furthermore, Kalibaeva *et al.* demonstrated that one can combine a novel update scheme for a particular set of velocity-dependent forces with SHAKE methodology for applying constraints [30]. Details of the procedure can be found in their paper. Taking into account the assumption that the simulation model is for the inertialess regime, one may also use an alternate method for evolving the system. Here we solve a purely dissipative Langevin equation. Inertial effects are eliminated by minimizing the inertial time-scale, with respect to all other times-scales, to the point where it does not influence the results. Details can be found in References [31] and [32].

III. COMPARISON TO SLENDER BODY THEORY

We want to evaluate the validity of using a collection of discrete Stokeslets to approximate the behavior of a continuous filament. Relevant analytical solutions that can be used for comparison are numbered, and only manageable in the regime of small deformation. Our comparison to theoretical results are likewise restricted to this regime. Cox, Batchelor, and Tillet carried out seminal theoretical work on a slender elastic body undergoing sedimentation, with which some comparisons can be made [33–35]. To compare our model with their results, let us first start with our definition of the hydrodynamic force, Eq. (7).

A. Average friction coefficient

Take the example of a filament experiencing a uniform external force density perpendicular to its axis, denoted by f^y ($= F_j^y/b$). Eq. (7) for this example is

$$F_{iH} = -\gamma_0 v_i + \frac{3af^y}{4}\left(\sum_{j=1}^{i-1}\frac{1}{j} + \sum_{j=1}^{n-i}\frac{1}{j}\right). \tag{8}$$

The sum in Eq. (8) can be estimated using the definition of the Euler-Mascheroni constant, k (≈ 0.5772).

$$k = \lim_{m\to\infty}\left(\sum_{j=1}^{m}\frac{1}{j} - \ln(m)\right) \tag{9}$$

Although this definition is for an infinite series, the following finite sum is a good approximation.

$$\sum_{j=1}^{m}\frac{1}{j} \approx \ln(m) + k \tag{10}$$

For instance, for $m = 100$, the highest order omitted term $(1/2m)$ in the harmonic series is already two orders of magnitude smaller than k. With this approximation, we can write Eq. (8) in terms of the dimensionless contour length, x ($= s/l$, where $s = jb$), spanning the interval $[-1, 1]$. The result is

$$F_H(x) = -\gamma_0 v(x) + \frac{3af^y}{4}\ln\left(\frac{1-x^2}{(\beta b/l)^2}\right), \tag{11}$$

where $\beta = e^{-k}$.

Consider the steady state solution, when the total hydrodynamic force matches the external force ($-F^y = F_H$). All sections of the filament move with the same velocity, the terminal or steady state velocity, which we label U. Using $L \approx nb$ for large n, we have

$$-bf^y = -\gamma_0 U + \frac{1}{L}\int_{-1}^{1}\left[\frac{3af^y}{4}\left(\ln\left(\frac{1-x^2}{(\beta b/l)^2}\right)\right)\right]dx. \tag{12}$$

The logarithmic term diverges at the ends but is integrable. The solution is

$$\gamma_0 U = F^y\left[\frac{b}{L} + \frac{3a}{2L}\left(\ln\left(\frac{L}{\beta b}\right) - 1\right)\right] \tag{13}$$

The average friction coefficient ($\gamma^\perp$) of sedimenting filament can be evaluated by taking the quotient of the total imposed external force and the resultant terminal velocity.

$$\gamma^\perp = \frac{F^y}{U} = \frac{4\pi\eta L}{\ln\left(L/(\beta b)\right) + \frac{2b}{3a} - 1} \tag{14}$$

From theory [33], the friction coefficient of a slender body is

$$\bar{\gamma}^\perp = \frac{4\pi\eta L}{\ln\left(L/r\right) + C_2} + O\left(\ln^{-3}(L/r)\right), \tag{15}$$

where C_2 depends on the cross sectional shape. For a uniform circular cross-section $C_2 = \ln(2) - 1/2$. When the filament radius is chosen to be $r = \beta b$ and the hydrodynamic radius is chosen to be $a^\perp = 4b/(3(2\ln 2 + 1)) \approx 0.559b$, our result is in exact agreement with theory (to the order of error in the equations) for the case of sedimentation perpendicular to the axis.

Starting with Eq. (7) and instead considering the scenario of the filament experiencing a uniform force density parallel to its axis, we find that the average friction coefficient is

$$\gamma^\parallel = \frac{2\pi\eta L}{\ln\left(L/(\beta b)\right) + \frac{b}{3a} - 1}. \tag{16}$$

From theory,

$$\bar{\gamma}^\parallel = \frac{2\pi\eta L}{\ln\left(L/r\right) + C_1} + O\left(\ln^{-3}(L/r)\right), \tag{17}$$

where C_1 is a coefficient that again depends on the cross sectional shape. For a uniform circular cross-section, $C_1 = \ln(2) - 3/2$. For the case of axial sedimentation, our results match theory exactly when $r = \beta b$ and $a^\parallel = 2b/(3(2\ln 2 - 1)) \approx 1.726b$.

B. Relationships between a, r, and b

In order for the Stokesian hydrodynamic treatment to be consistent with the results from slender body theory, the hydrodynamic and the filament radii must be chosen appropriately.

In the shish kebab model both a and r are chosen to be simply $b/2$ [20]. However, our analysis indicates that there is a more consistent choice.

First, we determined that the filament radius using the Stokesian treatment is $r = \beta b \approx 0.562b$, and therefore dictated by the degree of discretization. As the discretization increases, the bead spacing decreases, and the model mimics a more slender filament.

The more interesting result is that two hydrodynamic radii are recovered, one for motion perpendicular to the filament and one for motion parallel.

$$\begin{aligned} a^{\perp} &= \frac{4b}{3\left(2\ln(2)+1\right)} \approx 0.559b \\ a^{\parallel} &= \frac{2b}{3\left(2\ln(2)-1\right)} \approx 1.726b \end{aligned} \tag{18}$$

When a tensor hydrodynamic radius is implemented according to Eq. (18), the hydrodynamic force in the limit that the force mediated by the fluid is negligible reduces to resistive force theory with a tensor friction coefficient (since $\gamma_0^{\perp(\parallel)} = 6\pi\eta a^{\perp(\parallel)}$).

$$F_{iH} = -\left(\gamma_0^{\perp}\hat{\mathbf{n}}\hat{\mathbf{n}} + \gamma_0^{\parallel}\hat{\mathbf{p}}\hat{\mathbf{p}}\right)\cdot\mathbf{v}_i \tag{19}$$

The vector $\hat{\mathbf{n}}$ ($\hat{\mathbf{p}}$) is the unit direction normal (perpendicular) to the filament.

In studies using resistive force theory, a popular choice for the ratio of the *bead* friction coefficients is $\gamma_0^{\parallel}/\gamma_0^{\perp} = 1/2$, equivalent to the ratio of the *average* friction coefficients in the limit of an infinitely slender body. This is not the best choice. Finite slenderness must be accounted for. In our model the ratio of the *bead* friction coefficients is $\gamma_0^{\parallel}/\gamma_0^{\perp} \approx 3.09$. This is counterintuitive because the parallel friction coefficient of the filament is actually always lower than that perpendicular. But, as Sec. IV shows, the *average* friction coefficients for motion in each direction are recovered to a greater degree of accuracy using these values.

Given the effective radius for parallel movement is around three times that for perpendicular movement, the resultant hydrodynamic shape of the filament is caterpillar-like, having the basic features of an ordinary garden cabbage looper. Therefore, we refer to it as "caterpillar" Oseen hydrodynamics. An illustration of the hydrodynamic shape is shown in Figure 1.

C. Inhomogeneous hydrodynamic force

As a further confirmation that our results are consistent, there is an additional theoretical result with which we can compare: the (inhomogeneous) friction coefficient along the contour

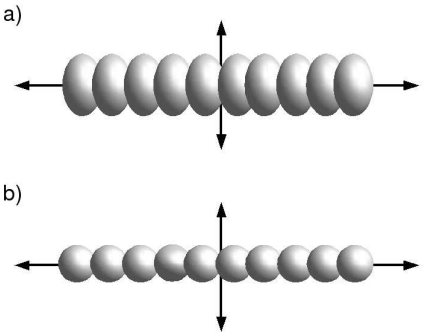

FIG. 1: A schematic of a) caterpillar and b) shish kebab hydrodynamic filament shapes.

length during sedimentation [33, 36]. The result for perpendicular sedimentation, rewritten in terms of the variable definitions in this paper, is

$$\frac{f^y}{2\pi\eta U} = -\frac{2}{\ln(\epsilon)} - \frac{1+2\ln(2)+\ln(1-x^2)}{\ln^2(\epsilon)} + O\left(\ln^{-3}(\epsilon)\right), \tag{20}$$

where the constant ϵ is the *slenderness parameter*, defined as $\epsilon = r/l$.

Defining $\tilde{\epsilon} = \beta b/l$, we can write the steady state friction from Eq. (11) as

$$\gamma_0 U = bf^y + \frac{3af^y}{4} \ln\left(\frac{1-x^2}{\tilde{\epsilon}^2}\right). \tag{21}$$

We expand Eq. (21) in terms of $\ln^{-1}(\tilde{\epsilon})$ to get

$$\frac{f^y}{2\pi\eta U} = -\frac{2}{\ln(\tilde{\epsilon})} - \frac{\frac{4b}{3a}+\ln(1-x^2)}{\ln^2(\tilde{\epsilon})} + O\left(\ln^{-3}(\tilde{\epsilon})\right). \tag{22}$$

This is equivalent to Eq. (20) when the following two conditions hold:

$$\tilde{\epsilon} = \epsilon \tag{23}$$

$$\frac{4b}{3a^\perp} = 1 + 2\ln(2). \tag{24}$$

Therefore, the filament radius is $r = \beta b$, and the effective hydrodynamic radius is $a^\perp = 4b/(3(2\ln 2 + 1))$. The analysis also holds for a comparison of the hydrodynamic force during parallel sedimentation.

These conclusions are consistent with those from the analysis in Sec. III A, where we calculated the average friction coefficient for sedimentation in the perpendicular direction. Confirmation that the correct inhomogeneous hydrodynamic force is recovered, even whilst neglecting higher order terms in Eq. (15), is significant since it is this variation in the hydrodynamic force that causes the deformation of the flexible body.

IV. RESULTS FROM SIMULATION

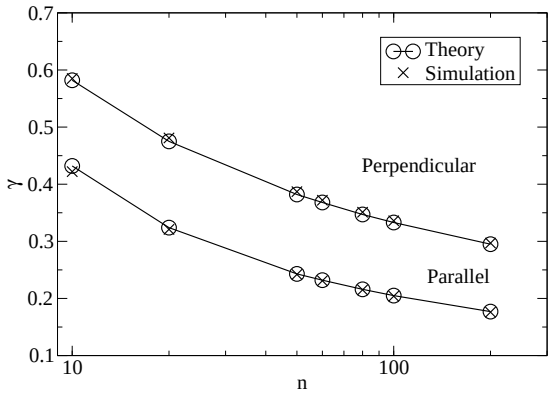

FIG. 2: Average friction coefficient versus bead density of a sedimenting filament in steady state using the caterpillar model ($B = 0.01$, $L = 1$), where $n = l/r$.

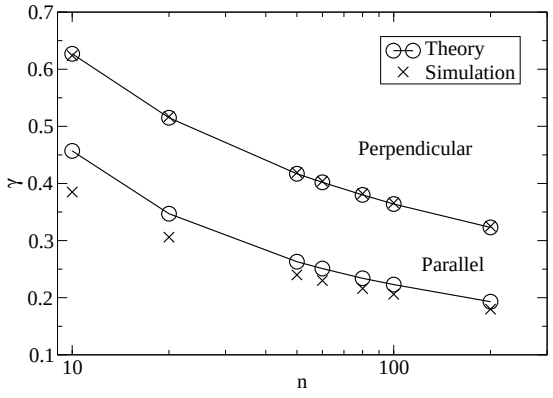

FIG. 3: Average friction coefficient versus bead density of a sedimenting filament in steady state using the shish kebab parameterization ($B = 0.01$, $L = 1$), where $n = l/r$.

To compare our computational model with slender body theory, a series of simulations was carried out. For all calculations, the starting configuration is a single filament oriented along the x-axis. The number of beads n (and the resultant filament slenderness) in this case is variable. Each pair of neighboring beads is constrained to be at a separation $b = L/(n-1)$. The velocity was initialized to zero. We introduce a dimensionless force

$$B = \frac{L^3 F}{\alpha}\,, \tag{25}$$

which weighs the relative magnitudes of the elastic and external forces. When $B \ll 1$, elastic forces dominate and the filament remains largely straight. When $B \gg 1$, the magnitude of the external forces is large enough for significant deformation to occur.

The test case we consider is a full dynamic simulation of sedimentation, both parallel and perpendicular to the primary axis of the filament. A uniform force density was applied to the system and the equations of motion integrated until the body reached a constant, terminal velocity. From this steady state configuration, we analyzed the forces. To give an idea of the computational cost, a typical simulation of a filament modeled with 80 beads takes about an hour on a computer with an Intel Pentium D processor (3.00 GHz) running Fedora Linux. To allow comparison with theory the magnitudes of the external force density and the flexure were chosen such that the deflection amplitude is small (well within one percent of the length) in the steady state configuration. In terms of the dimensionless force, all simulations were carried out with $B \leq 0.01$. For the model this is not a necessary restriction, the high B regime can also be studied. The length L for all simulations was set to unity.

The average friction coefficients calculated from our simulations are plotted in Figure 2 along with the theoretical values from Eq.'s (15) and (17). Our model shows excellent agreement to theory, even for the very smallest bead density of $n/L = 10$. In contrast, calculations using the shish kebab parameterization are plotted in Figure 3. The values for the case of sedimentation perpendicular to the axis are reproduced accurately because the hydrodynamic radius is chosen to be $a = b/2$, which is very close to our value of $a^{\perp} = 0.559b$. The average friction coefficient that results from motion parallel to the axis, however, only matches in the limit that the body is infinitely slender. The results in the limit of realistic cross-section differ substantially from theory. The discrepancy is over 15% for the lowest aspect ratio considered ($n/L = 10$).

We also compare the inhomogeneous friction coefficient as a function of contour length that was introduced in Sec. III C. The analytical expression (Eq. (20)) and results from simulation are plotted in Figure 4. They show excellent agreement overall. The slight deviation is due to the fact that we are comparing our model to only the leading order term from theory, although our simulation results contain higher order contributions. The higher order terms appear to have little cumulative effect on the average friction coefficient results in Figure 2.

Xu and Nadim extended the groundwork of Cox, Batchelor, and Tillett and determined

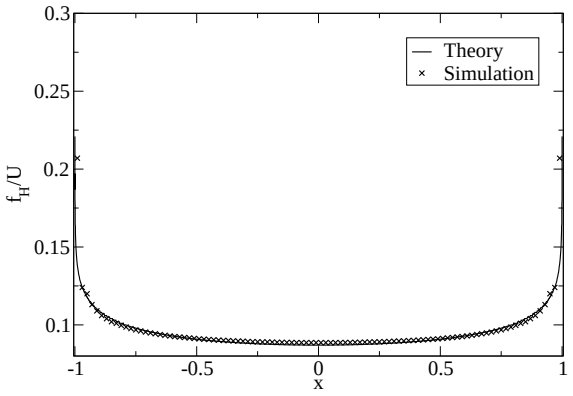

FIG. 4: Friction coefficient from theory and simulation for n/L=100 and B=0.01.

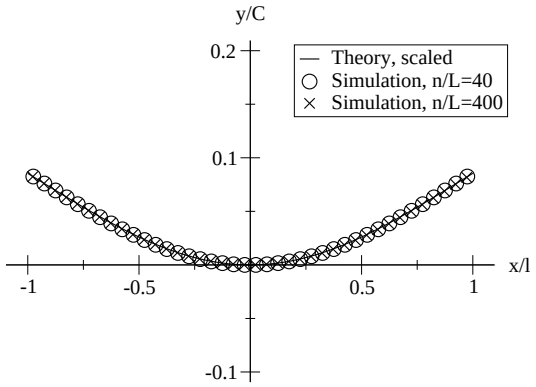

FIG. 5: Dimensionless deflection as a function of contour length.

an expression for the y-deflection by solving the differential equation of beam deflection from elasticity theory by using the appropriate Green's function [13]. From Eq. (7) in their article, the deflection is given by

$$y(x) = -\frac{C}{24}\left[(1+x)^4\ \ln(1+x) + (1-x)^4\ \ln(1-x) - \left(\frac{13}{6} + 2\ \ln 2\right) x^4 - (1 + 12\ \ln 2)\, x^2\right]. \tag{26}$$

Please note that there is a typographical error in the original paper that has been corrected here [37]. The constant C is

$$C = \frac{2\pi\eta U l^4}{EI \ln^2(\epsilon)}, \tag{27}$$

where EI is the Young's modulus times the second moment of area, which together constitute the beam flexure α. The ranges of the parameters for which the deflection was calculated

are $B = 10^{-5} - 10^{-1}$ and $n/L = 20 - 400$. All parameter sets investigated yielded the same dimensionless deflection. Two representative data sets are plotted in Figure 5. When the theoretical dimensionless deflection is scaled by a constant factor of approximately 1.15, the theory matches our simulation. The modest discrepancy is most likely due to the omission of higher order terms in the derivation of Eq. (26), terms that our simulation model does include. It is significant to note that both the theoretical and simulation results agree in the prediction that the functional form of the deflection is independent of slenderness.

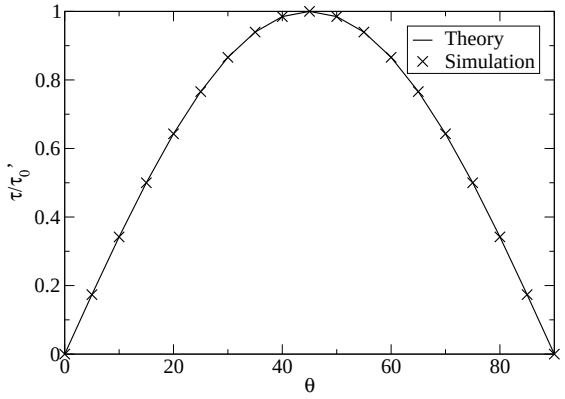

FIG. 6: Normalized torque as a function of θ, the angle between the filament end-to-end vector and the plane orthogonal to the force axis.

Xu *et al.* also derived an expression for the torque acting on a flexible slender body. The torque will cause the filament to rotate during sedimentation until a final orientation is achieved in which the filament's centerline is perpendicular to the force axis. Their result is

$$T = C_T \frac{2\pi^2 \eta^2 U^2 l^5 \sin(2\theta)}{EI \ln^4(\epsilon)} = \tau_0 \sin(2\theta). \tag{28}$$

The variable θ is the angle between the filament axis and $\hat{x}$ when the external force is applied in the $\hat{y}$ direction. C_T is

$$C_T = \int_0^1 y(x) \left[2\ln 2 - 2 - \ln\left(1 - x^2\right)\right] dx \approx 0.01661, \tag{29}$$

calculated by numerical integration. The normalized torque as a function of θ is plotted in Figure 6 along with the theoretical functional dependence. For the functional forms the results are in excellent agreement. However, the normalization constant τ_0' from Figure 6 is different from τ_0 from theory. This is expected since the y-deflection from our simulation results differs slightly from the analytic result that was used in the derivation of Eq. (28).

V. DISCUSSION AND CONCLUSIONS

We described a simulation model for an elastic filament that accurately accounts for intra-filament hydrodynamic interactions. We showed that the discrete Stokesian treatment encapsulates the physics of a continuous filament of finite cross-section when a specific tensor bead friction is chosen. Furthermore, in the limit that the inhomogeneity in the friction coefficient is neglected, the caterpillar model reduces to simple resistive force theory with a tensor bead friction coefficient. It follows from our analysis that the bead spacing dictates the local radius of the filament. Therefore, when the two consecutive beads are not constrained but instead connected by a simple spring, the inter-bead distance and therefore the resultant filament radius is variable [18, 19]. By applying length constraints to the inter-bead distance, as we do in this model, the radius is constant along the contour length of the filament, which is a more realistic description.

The caterpillar model accurately simulates the dynamics of filament sedimentation for all aspect ratios considered, whereas the shish kebab parameterization only recovers the correct average friction coefficients for an infinitely slender body (infinitely high bead density). A *real* filament is not infinitely slender but has a diameter that may be a few percent of the filament length [1, 2]. There is significant deviation from the correct hydrodynamic behavior in this regime using the shish kebab parameterization.

Our simulation results for the dimensionless deflection of a filament sedimenting perpendicular to its axis agree with the theoretical prediction that the steady state shape does not depend on the slenderness of the filament. Also, calculations of the torque acting on a mis-aligned filament support that the functional dependence is $\sin(2\theta)$. We observed a modest discrepancy in the magnitude of the dimensionless deflection between our simulations and the theoretical results. This could be due to the omission of higher order terms in the derivation of the theoretical result. Another potential source of the difference may be that the theoretical deflection (Eq. 26) is calculated from a differential equation that does not include a Lagrange multiplier to enforce constant length. Our simulation model is a slightly different description in that no energy can be stored in the axial direction.

We have chosen the hydrodynamic radius specifically to recover the results of a body with a uniform circular cross-section. But, it is possible to choose it instead to match the average parallel and perpendicular friction coefficients for a different cross-sectional radius

profile [33]. One simply has to use different values for the constants C_2 and C_1 in Equations (15) and (17), respectively. This means that the dynamic response actually depends on the specific geometry considered. We chose a uniform circular cross-section because it is a realistic representation for the shape for microtubules, nanotubes, and cilia/flagella of fabricated micro-swimmers.

Where might this model be relevant? The ratio of the two friction coefficients is particularly important in the field of micro-organism motility. The swimming speed (and thrust) of a flagella with planar waves, for instance, is proportional to $(1 - \gamma^{\parallel}/\gamma^{\perp})$ [3]. Any deviation in this ratio will have significant effects on the motility. In the extreme case where $\gamma^{\parallel} = \gamma^{\perp}$, the organism cannot move at all!

Elastic, hydrodynamic, and tension forces form the basis for the model. However, incorporating other forces is trivial. Biological molecules are frequently charged. With this model, one could investigate the dynamics of a charged filament such as a microtubule in an electric field, for example [6, 7]. The scope of problems one can investigate using the deterministic simulation model presented here, in which thermal fluctuations are neglected, is delineated by the condition that the time scale of diffusion is significantly longer than the time scale associated with the motion of interest. In practice this restricts its applicability to relatively stiff filaments. Nonetheless, similar considerations of parameterizing the Stokeslet hydrodynamic description apply when one includes thermal fluctuations. Such a model can then address an even wider class of important problems, notably the dynamics of DNA fragments.

We thank Prof. A. Nadim for helpful discussions. A.G.B. thanks the Thouron Award, NSF Graduate Research Fellowship Program, and the Thomas Young Centre Junior Research Fellowship program for support. I.P. acknowledges financial support from MICINN (Project FIS2008-04386).

---

[1] E. M. Purcell, Am. J. Phys. **45**, 3 (1977).

[2] G. J. Hancock, Proc. R. Soc. Lond. A **217**, 96 (1953).

[3] C. Brennen and H. Winet, Annu. Rev. Fluid Mech. **9**, 339 (1977).

[4] D. Smith, E. Gaffney, and J. Blake, B. Math. Biol. **69**, 1477 (2007).

[5] R. Dreyfus, J. Baudry, M. Roper, M. Fermigier, H. Stone, and J. Bibette, Nature **437**, 862 (2005).

[6] M. van den Heuvel, M. de Graaff, S. Lemay, and C. Dekker, Proc. Natl. Acad. Sci. (USA) **104**, 7770 (2007).

[7] M. van den Heuvel, R. Bondesan, M. Cosentino Lagomarsino, and C. Dekker, Phys. Rev. Lett. **101**, 118301 (2008).

[8] C. P. Lowe, Phil. Trans. Roy. Soc. London. B **358**, 1543 (2003).

[9] I. Llopis, I. Pagonabarraga, M. Cosentino Lagomarsino, and C. P. Lowe, Phys. Rev. E **76**, 061901 (2002).

[10] G. Alexander, C. Pooley, and J. Yeomans, Phys. Rev. E. **78**, 045302(R) (2008).

[11] J. Gray and G. J. Hancock, J. Exp. Biol. **32**, 802 (1955).

[12] M. Cosentino Lagomarsino, I. Pagonabarraga, and C. P. Lowe, Phys. Rev. Lett. **94**, 148104 (2005).

[13] X. Xu and A. Nadim, Phys. Fluids **6**, 2889 (1994).

[14] M. J. Shelley and T. Ueda, Physica D **146**, 221 (2000).

[15] R. E. Goldstein and S. A. Langer, Phys. Rev. Lett. **75**, 1094 (1995).

[16] R. E. Goldstein, T. R. Powers, and C. H. Wiggins, Phys. Rev. Lett. **80**, 5232 (1998).

[17] L. E. Becker and M. J. Shelley, Phys. Rev. Lett. **87**, 198301 (2001).

[18] Y. Kim and R. Netz, Phys. Rev. Lett. **96**, 158101 (2006).

[19] X. Schlagberger and R. Netz, Phys. Rev. Lett. **98**, 128301 (2007).

[20] M. Doi and S. F. Edwards, *The Theory of Polymer Dynamics* (Oxford University Press, Oxford, UK, 1986).

[21] L. Landau and E. Lifshitz, *Theory of elasticity* (Butterworth-Heinemann, Boston, MA, 1986), 3rd ed.

[22] O. Kratky and G. Porod, Rec. Trav. Chim. Pays-Bas **68**, 1106 (1973).

[23] M. Fixman and J. Kovac, J. Chem. Phys. **58**, 1564 (1973).

[24] S. B. Smith, L. Finzi, and C. Bustamante, Science **258**, 1122 (1992).

[25] J. Marko and E. Siggia, Macromolecules **28**, 8759 (1995).

[26] J.-P. Ryckaert, G. Ciccotti, and H. J. C. Berendsen, J. Comput. Phys. **23**, 327 (1977).

[27] A. G. Bailey, C. P. Lowe, and A. P. Sutton, J. Comput. Phys. **227**, 8949 (2008).

[28] W. C. Swope, H. C. Andersen, P. H. Berens, and K. R. Wilson, J. Chem. Phys. **76**, 6548

(1982).

[29] M. Tuckerman, B. J. Berne, and G. J. Martyna, J. Chem. Phys. **97**, 1990 (1992).

[30] G. Kalibaeva, M. Ferrario, and G. Ciccotti, Mol. Phys. **101**, 765 (2003).

[31] R. Argentini, Ph.D. thesis, Universiteit van Amsterdam (2008).

[32] C. P. Lowe, Future Gener. Comp. Sy. **17**, 853 (2001).

[33] R. G. Cox, J. Fluid Mech. **44**, 791 (1970).

[34] G. K. Batchelor, J. Fluid Mech. **44**, 419 (1970).

[35] P. K. Tillett, J. Fluid Mech. **44**, 401 (1970).

[36] J. B. Keller and S. I. Rubinow, J. Fluid Mech. **75**, 705 (1976).

[37] We are grateful to Prof. A. Nadim for pointing this out to us.